Properties of Steady States in Turbulent Axisymmetric Flows

R. Monchaux,* F. Ravelet, B. Dubrulle, A. Chiffaudel, and F. Daviaud

Service de Physique de l'État Condensé, DSM, CEA Saclay, CNRS URA 2464, 91191 Gif-sur-Yvette, France

(Received 19 September 2005; published 29 March 2006)

We experimentally study the properties of mean and most probable velocity fields in a turbulent von Kármán flow. These fields are found to be described by two families of functions, as predicted by a recent statistical mechanics study of 3D axisymmetric flows. We show that these functions depend on the viscosity and on the forcing. Furthermore, when the Reynolds number is increased, we exhibit a tendency for Beltramization of the flow, i.e., a velocity-vorticity alignment. This result provides a first experimental evidence of nonlinearity depletion in nonhomogeneous nonisotropic turbulent flow.

DOI: 10.1103/PhysRevLett.96.124502 PACS numbers: 47.27.E−, 05.70.Ln

Introduction.—A yet unanswered question in statistical physics is whether stationary out-of-equilibrium systems share any resemblance with classical equilibrium systems. A good paradigm to explore this question is offered by turbulent flows. Incompressible flows subject to statistically stationary forcing generally reach a steady state, in a statistical sense, independent of the initial conditions. Most of the current turbulence modeling is devoted to the understanding of this state, and the role of the velocity fluctuations or velocity smallest scales in its construction. A distinguished feature of stationary large Reynolds number turbulent flows is the presence of coherent structures, under the shape of vortices in 2D [1,2], or vorticity thin tubes in 3D [3]. These structures correspond to regions where vorticity is locally almost aligned with velocity—phenomenon referred to as Beltramization [4,5]. This tendency to velocity-vorticity alignment induces depletion of nonlinearities in Navier-Stokes equations. Interestingly enough, similar depletion of nonlinearity is also observed in the inviscid counterpart of the Navier-Stokes equation—the so-called Euler equation—resulting in a slowing down of the vorticity blowup with respect to rigorous estimates [6]. A theoretical question of interest is therefore whether turbulent flows have a natural tendency for nonlinearity depletion, and whether this is a characteristic of the steady states.

The answer to the first issue is ambiguous. On one hand, a tendency for Beltramization has indeed been observed in some numerical simulations of stationary, nearly isotropic turbulence [7,8]. On the other hand, similar studies performed on more general flows—such as boundary layer [9]—provided little evidence of such a property. A similar conclusion has been reached using experimental data [10], with slightly less reliability owing to the difficulty to measure vorticity. As for the second issue, it has only been partially explored in special geometries. In 2D, equilibrium states of the Euler equations have been classified through statistical mechanics principle by Robert and his collaborators [11,12]. They indeed correspond to Beltrami solution. In 3D axisymmetric flows—an intermediate situation between 2D and 3D—a similar task has been undertaken by Leprovost *et al.* [13]. In the ideal case—force free, inviscid—they proved the existence of an infinite number of conserved quantities, in addition to the energy and the helicity. They also showed the existence of an infinite number of equilibrium states, depending on the conserved quantities. Among them, a Beltrami state is obtained, when only the energy and the helicity are conserved. They postulated that even in the presence of small but finite viscosity and forcing [14], this feature remains valid, with selection of steady states through boundary conditions and forcing.

The purpose of this Letter is to perform an experimental check of these findings. We find that mean and most probable velocity fields of axisymmetric flows can indeed be characterized by two families of functions, as predicted in Ref. [13]. These functions depend on the viscosity and forcing. As the Reynolds number is increased, they evolve toward the functions corresponding to a Beltrami state, providing a first evidence of nonlinearity depletion in a nonhomogeneous, nonisotropic system.

Theoretical background and definitions.—Consider an incompressible axisymmetric flow, with velocity components in a cylindrical referential (v_r, v_θ, v_z). Because of incompressibility and axisymmetry, only two functions are sufficient to describe the flow, namely, the angular momentum—$\sigma(r, z) = r v_\theta$—and either the stream function $\Psi(r, z)$, such that $(v_r, v_z) = -\nabla \times \Psi e_\theta$, or the azimuthal vorticity $\omega_\theta(r, z)$. Using a variational method, Leprovost *et al.* showed that the steady states solution of axisymmetric Euler equations, in the force-free case obey

$$\sigma = F(\Psi); \qquad \xi - \frac{FF'}{r^2} = G(\Psi); \qquad \text{with } \xi = \omega_\theta / r, \tag{1}$$

where F and G are arbitrary functions linked with conservation laws of the system—Casimirs of σ, generalized helicity [13]. For example, the steady state corresponding to conservation of energy and helicity is such that F is linear and $G \equiv 0$, resulting in a linear relation between vorticity and velocity ($\vec{v} = \lambda \vec{\omega}$). This is a Beltrami flow, given by

$$v_r = -\frac{\pi R}{Hm} J_1\left(m\frac{r}{R}\right)\cos\left(\pi\frac{z}{H}\right),$$
$$v_\theta = \frac{\lambda R}{m} J_1\left(m\frac{r}{R}\right)\sin\left(\pi\frac{z}{H}\right), \quad (2)$$
$$v_z = J_0\left(m\frac{r}{R}\right)\sin\left(\pi\frac{z}{H}\right),$$

where λ and m are free parameters and J_0 and J_1 are first order Bessel functions.

Considering further the thermodynamics of the system, Leprovost *et al.* proved that the equilibrium states at some fixed coarse-grained scale are such that the most probable velocity flow (MPVF) is a stationary state of the Euler equation, i.e., satisfies Eq. (1). Finally, they postulated that these force-free, inviscid results can be extended to the stationary states in the presence of both viscosity and forcing, providing the function F and G are selected through boundary conditions and forcing.

Experimental setup.—In order to check the theoretical predictions, we have worked with a simple "axisymmetric" configuration: the von Kármán flow generated by two counter-rotating impellers in a cylindrical vessel. The cylinder radius and height are, respectively, $R = 100$ mm and $H = 180$ mm (distance between inner faces of impellers). The impellers consist of 185 mm diameter disks fitted with sixteen 20 mm high curved blades. More details about the experimental setup can be found in Ref. [15]. The impellers' rotation frequencies are both set equal to f to get exact counter-rotating regime. We define two forcing associated with the concave [convex] face of the blades going forward, denoted in the sequel by direction $(-)$ $[+]$. The working fluid is either water or glycerol at different dilution rates. The resulting accessible Reynolds numbers ($\mathrm{Re} = 2\pi f R^2 \nu^{-1}$ with ν the kinematic viscosity) vary from 10^2 to 3×10^5. In the exact counter-rotating regime, whatever the impellers, the flow is divided into two toric cells separated by an azimuthal shear layer. This setup is invariant under rotations of π ($\mathcal{R}_\pi$) around any radial axis passing through the center of the cylinder. The time-averaged velocity fields we consider hereafter are $\mathcal{R}_\pi$ invariant and axisymmetric [15]. Velocity measurements are done with a DANTEC laser doppler velocimetry (LDV) system.

Data processing.—The LDV data only provide the axial and azimuthal velocity components on a 170 point grid covering half a meridian plane, through time series of about 200 000 randomly sampled values at each grid point. From this time series, it is straightforward to get time-averaged axial and azimuthal velocities. The remaining radial component of the mean velocity field can then be obtained using the incompressibility and axisymmetry: this procedure has been later validated through direct measurements of the radial velocity with a particles image velocimetry system on the same flow. We also use the time series to extract at each point histograms of the axial and azimuthal velocity, and compute the flow of most probable velocities (FMPV) [16], obtained by taking, at each point, the most probable value of the velocity. The v_r component is once more derived from the two other components using continuity equation. Figure 1 compares the two flows computed from the same data set: they have the same overall structure, but differ through the size of the middle shear layer, which is thinner in the case of the FMPV. This is due to the fact that the chaotic wandering of the shear layer around its average position is significantly less probable as one considers positions further away from the equatorial plane. From a theoretical point of view, the two flows differ in the sense that the mean velocity is not a solution of the Navier-Stokes or Euler equations—because of the fluctuations, which induce a Reynolds stress, especially in the shear layer—while the MPVF is a stationary solution of the Euler equations. Therefore, one can expect theoretical predictions regarding the structure of the stationary state to be less accurate in the case of the mean flow, as the Reynolds number and the fluctuations increase.

We first compute the F function by looking at σ as a function of Ψ, and then we use this estimate to evaluate G, by looking at $\xi_2 = \xi - \frac{FF'}{r^2}$ as a function of Ψ. This procedure is likely to induce a lot of noise in the estimate of G. To check its robustness, we have tested it on a Beltrami flow [Eq. (2)] with a superimposed level of noise comparable to the level of fluctuations in the flow (see Fig. 2). Even in the presence of noise the fits give the correct shapes: $F = \lambda\Psi$ and $G \equiv 0$.

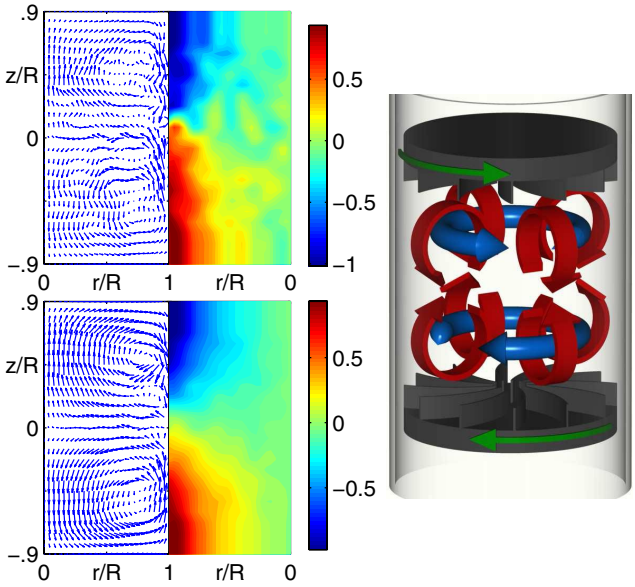

FIG. 1 (color online). Velocity profile for $\mathrm{Re} = 2.5 \times 10^5$, direction $(-)$: colored contour for azimuthal component, arrow representation for poloidal part. Top: FMPV. Bottom: time-averaged flow. Right part displays a sketch of the two toric recirculating cells.

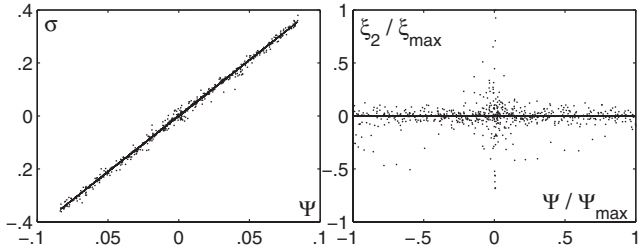

FIG. 2. σ and $\xi_2 = \xi - \frac{FF'}{r^2}$ versus Ψ for the Beltrami flow defined by Eq. (2) with a superimposed white noise of amplitude 60%. We have represented the F and G fits on, respectively, the left and right figures.

After this test, we apply this procedure on the real data, with a further correction, motivated by the following remark. Figure 3 displays two typical plots of F: one over the whole apparatus, and one over a 50% portion of the flow obtained after removing regions close to the impellers and along the vessel. These parts correspond to locations where the viscosity and the forcing (neglected in Ref. [13]) are principally at work, and larger deviations from theoretical predictions can be expected. One sees that while data on the whole vessel display significant scatter, preventing the outcome of a well-defined F, the restricted data gather onto a cubic-shaped function fitted by a two parameters cubic: $F(\Psi) = p_1\Psi + p_3\Psi^3$. This fit is then used to obtain G. In the sequel, we obtain F and G through fits over this 50% portion of the flow away from the boundaries.

Results.—We present results computed for both time-averaged flow and FMPV for the two directions of rotation, at different Reynolds numbers. Figure 4 presents the F fits obtained in each case. We have included on each graph a straight line tangent to experimental curves for $\Psi = 0$ as a reference to a Beltrami flow. The experimental data are much more scattered in the FMPV case, debasing the fit accuracy compared to the mean flow—$R^2 \simeq 0.94$ instead of 0.99.

In Fig. 5 we present the G fits obtained in the same conditions. The best fit of the FMPV G functions is linear, whereas cubic-shaped functions are required for time-averaged G. The plots of G consist of wide noisy bands

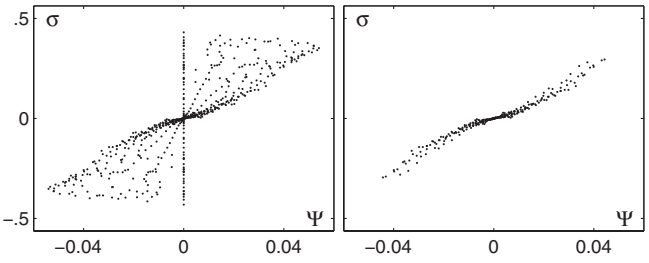

FIG. 3. σ vs Ψ for experimental time-averaged flow in direction (+) at Re = 2100. Left: for the whole flow. Right: for $r \leq 0.81$, $-0.56 \leq z \leq 0.56$, corresponding to 50% of the flow volume. The remaining points are clearly gathering along a cubic-shaped function F.

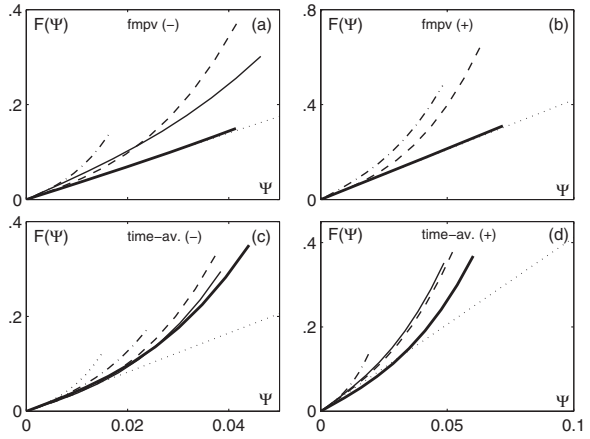

FIG. 4. F fit. (a) and (b) FMPV direction (−) and (+), respectively; (c) and (d) time-averaged field direction (−) and (+), respectively. Legend for all figures: Re = 100 (thin dotted line), Re = 150 (thin dot-dashed line), Re = 2100 (thin dashed line), Re = 9100 (thin solid line), Re = 2.5×10^5 (thick solid line). The thin dotted straight line is a Beltrami. As F is odd, we display it for positive values of Ψ only. Note that the fit at Re = 9100 for FMPV case in direction (+) could not be obtained from the data due to large scattering.

surrounding the fits in both cases. The noise for G is larger than for F, since it is a result of a two-step procedure including a spatial derivation.

Considering the variation with Reynolds number of F, both the FMPV case and the time-averaged case behave similarly. As Reynolds number increases, the F cubic curves collapse on the Beltrami line.

At Re = 2.5×10^5, it is not even possible to distinguish the F fit from a straight line and this for the two directions of rotation. In the case of G, there is a difference between the two cases. For the FMPV, the best fit is linear, with a slope smaller than the noise level; this is consistent with $G \equiv 0$. For the time-averaged case, the shape of G is very

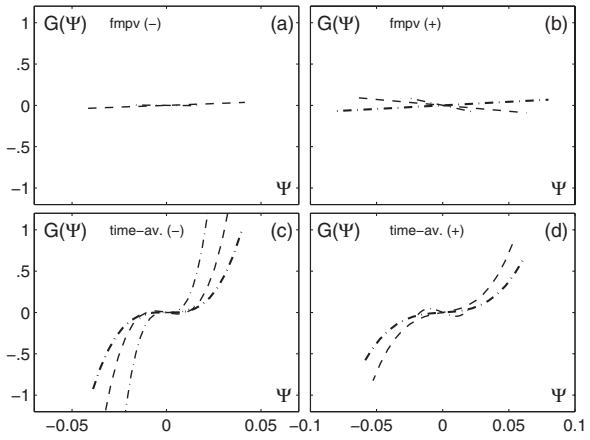

FIG. 5. G fit. (a) and (b) FMPV direction (−) and (+), respectively; (c) and (d) time-averaged field direction (−) and (+), respectively. Same legend as Fig. 4.

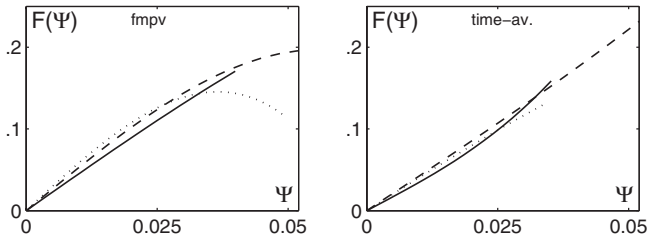

FIG. 6. F fit for 100 mm diameter impellers fitted with straight blades. Left: FMPV, Right: time-averaged. Re $= 1.9 \times 10^5$ (dotted line), Re $= 2.6 \times 10^5$ (dashed line), Re $= 5 \times 10^5$ (solid line).

different. All the fits present a *plateau* around zero. The greater the Reynolds number, the wider this *plateau*, so the wider the range of Ψ—or equivalently the volume of considered flow—where G is very close to zero, i.e., very close to the Beltrami G function.

The difference in the shape of G can be explained as follows: according to Eq. (1), $G(\Psi)$ is the difference of two terms. One linked to F is necessarily a cubic, while the second, connected to the azimuthal vorticity is almost a noise in this area of the flow. In the FMPV case, the magnitude of the cubic term is small compared to the vorticity, and we only see the noise coming from the vorticity. In the time-averaged case, the cubic is much larger, so that it determines the behavior of G.

A second observation is the dependence of F and G on the forcing. Comparison of Figs. 4(a) and 4(c) with 4(b) and 4(d) obtained for two different forcing, shows that the slope of F slightly depends on the forcing [$p_1 = 5$ for $(-)$ direction; $p_1 = 4$ for $(+)$ direction]. For any forcing, G remains close to zero at the measurement scale. To check this dependence further, we have conducted an additional experiment at high Reynolds number, with much smaller impellers. As shown in Fig. 6, we obtained a different shape for F, with a different inflection.

Discussion and perspectives.—An inviscid force-free theory developed by Leprovost *et al.* predicted a characterization of the steady state in axisymmetric turbulent flows through two functions F and G. In our experiments, we have confirmed this, and measured these functions for different forcing, and different viscosities, using two different fields as diagnostic: the FMPV as predicted and more surprisingly the time-averaged field, even in a region where Reynolds stresses are not negligible. This could be due to the quasi-Gaussian distributions of velocities.

First, we have observed that the functions are well-defined only in the portion of the flow remote from the boundaries, where forcing and dissipation take place. The steady states of the von Kármán flow can be described by these two functions, as predicted by a statistical analysis of equivalent equilibrium states assuming zero viscosity and no forcing [13]. Nevertheless, we have seen that forcing and dissipation do influence the steady state regime through the selection of the characteristic functions. Specifically, we have observed that the forcing selects the specific shape of the functions (linear, cubic, ...), while dissipation acts as a sort of self-similar zoom and select the portion of the curve actually explored by the flow. This suggests that stationary out-of-equilibrium systems like turbulent flows are universal in a weaker sense than in ordinary equilibrium systems: they can be described in a universal manner through general functions (like F and G) determining the "equation of state." However, these functions are nonuniversal since they depend on the fine details of the system (dissipation and forcing).

Finally, we have shown that the evolution for increasing Reynolds number is towards a Beltrami state, with depletion of nonlinearities. This evolution is more obvious when considering the FMPV, as expected from the thermodynamics analysis developed by Leprovost *et al.*. To our knowledge, this is the first experimental evidence of nonlinearity depletion in a nonhomogeneous, nonisotropic turbulence, where it is very challenging to measure simultaneously all components of velocity and vorticity. Our use of the functions characterizing the steady states enables us to lower the experimental constraints for such a check.

*Electronic address: romain.monchaux@cea.fr

[1] C. Basdevant, B. Legras, R. Sadourny, and M. Béland, J. Atmos. Sci. **38**, 2305 (1981).
[2] J. C. McWilliams, J. Fluid Mech. **219**, 361 (1990).
[3] A. Vincent and M. Meneguzzi, J. Fluid Mech. **225**, 1 (1991).
[4] R. Benzi *et al.*, J. Phys. A **19**, 3771 (1986).
[5] M. Farge *et al.*, Phys. Fluids **15**, 2886 (2003).
[6] P. Constantin and C. Fefferman, Indiana Univ. Math. J. **42**, 775 (1993).
[7] E. D. Siggia and G. S. Patterson, J. Fluid Mech. **86**, 567 (1978).
[8] R. B. Pelz, V. Yakhot, and S. A. Orszag, Phys. Rev. Lett. **54**, 2505 (1985).
[9] M. M. Rogers and P. Moin, Phys. Fluids **30**, 2662 (1987).
[10] J. M. Wallace, J.-L. Balint, and L. Ong, Phys. Fluids A **4**, 2013 (1992).
[11] J. Sommeria and R. Robert, J. Fluid Mech. **229**, 291 (1991).
[12] P. H. Chavanis, Phys. Rev. E **68**, 036108 (2003).
[13] N. Leprovost, B. Dubrulle, and P. H. Chavanis, physics/0505084 [Phys. Rev. E (to be published)].
[14] Considering the $\nu = 0$ and $\nu \to 0$ limit is different.
[15] F. Ravelet, L. Marié, A. Chiffaudel, and F. Daviaud, Phys. Rev. Lett. **93**, 164501 (2004).
[16] *A priori*, FMPV and MPVF are different. Experimentation only gives access to FMPV. Nevertheless, both may be quite similar if the velocity probability density function at each point shows a well-defined peak.